Journal Pre-proof

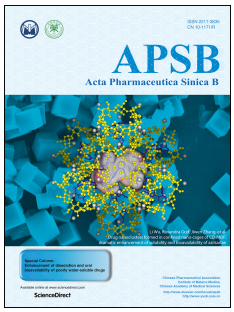

Repurposing of berbamine hydrochloride to inhibit Ebola virus by targeting viral glycoprotein

Dongrong Yi, Quanjie Li, Han Wang, Kai Lv, Ling Ma, Yujia Wang, Jing Wang, Yongxin Zhang, Mingliang Liu, Xiaoyu Li, Jianxun Qi, Yi Shi, George F. Gao, Shan Cen

PII: S2211-3835(22)00245-3

DOI: https://doi.org/10.1016/j.apsb.2022.05.023

Reference: APSB 1422

To appear in: *Acta Pharmaceutica Sinica B*

Received Date: 14 March 2022

Revised Date: 7 May 2022

Accepted Date: 12 May 2022

Please cite this article as: Yi D, Li Q, Wang H, Lv K, Ma L, Wang Y, Wang J, Zhang Y, Liu M, Li X, Qi J, Shi Y, Gao GF, Cen S, Repurposing of berbamine hydrochloride to inhibit Ebola virus by targeting viral glycoprotein, *Acta Pharmaceutica Sinica B*, https://doi.org/10.1016/j.apsb.2022.05.023.

Original article

Repurposing of berbamine hydrochloride to inhibit Ebola virus by targeting viral glycoprotein

Dongrong Yi[a,†], Quanjie Li[a,†], Han Wang[b,†], Kai Lv[a], Ling Ma[a], Yujia Wang[a], Jing Wang[a], Yongxin Zhang[a], Mingliang Liu[a], Xiaoyu Li[a], Jianxun Qi[b], Yi Shi[b,c,*], George F. Gao[b,c], Shan Cen[a,d,*]

[a]*Institute of Medicinal Biotechnology, Chinese Academy of Medical Sciences and Peking Union Medical School, Beijing 100050, China*

[b]*CAS Key Laboratory of Pathogenic Microbiology and Immunology, Institute of Microbiology, Chinese Academy of Sciences, Beijing 100101, China*

[c]*University of Chinese Academy of Sciences, Beijing 100049, China*

[d]*CAMS Key Laboratory of Antiviral Drug Research, Institute of Medicinal Biotechnology, Peking Union Medical College, Chinese Academy of Medical Sciences, Beijing 100050, China*

Received 14 March 2022; received in revised form 7 May 2022; accepted 12 May 2022

[*]Corresponding authors.

E-mail addresses: shancen@imb.pumc.edu.cn (Shan Cen), shiyi@im.ac.cn (Yi Shi).

[†]These authors made equal contributions to this work.

Running title: Inhibition of EBOV infection by berbamine hydrochloride

Graphical abstract

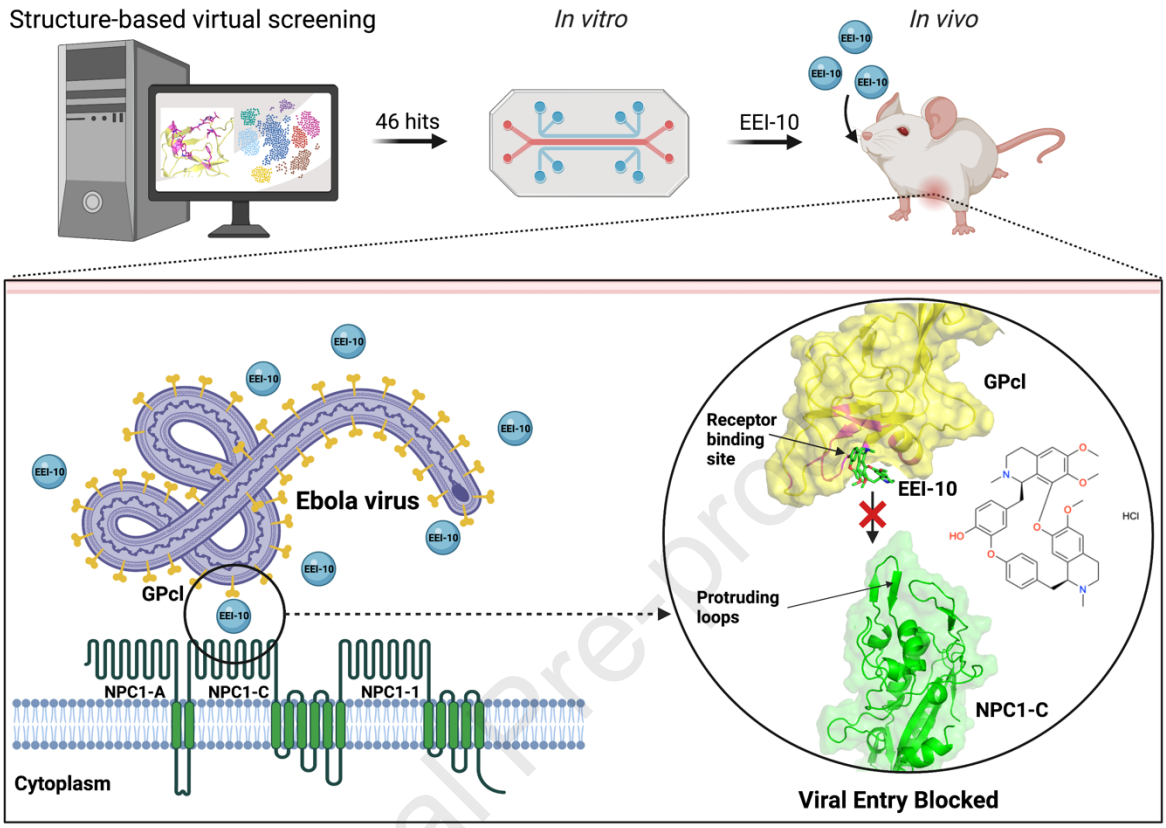

Through structure-based virtual screening, this study reported that a natural compound berbamine hydrochloride can disrupt GPcl–NPC1 interaction, and strongly inhibited EBOV replication *in vitro* and *in vivo*.

Original article

Repurposing of berbamine hydrochloride to inhibit Ebola virus by targeting viral glycoprotein

Dongrong Yi[a,†], Quanjie Li[a,†], Han Wang[b,†], Kai Lv[a], Ling Ma[a], Yujia Wang[a], Jing Wang[a], Yongxin Zhang[a], Mingliang Liu[a], Xiaoyu Li[a], Jianxun Qi[b], Yi Shi[b,c,*], George F. Gao[b,c], Shan Cen[a,d,*]

[a]*Institute of Medicinal Biotechnology, Chinese Academy of Medical Sciences and Peking Union Medical School, Beijing 100050, China*

[b]*CAS Key Laboratory of Pathogenic Microbiology and Immunology, Institute of Microbiology, Chinese Academy of Sciences, Beijing 100101, China*

[c]*University of Chinese Academy of Sciences, Beijing 100049, China*

[d]*CAMS Key Laboratory of Antiviral Drug Research, Institute of Medicinal Biotechnology, Peking Union Medical College, Chinese Academy of Medical Sciences, Beijing 100050, China*

Received 14 March 2022; received in revised form 7 May 2022; accepted 12 May 2022

[*]Corresponding authors.

E-mail addresses: shancen@imb.pumc.edu.cn (Shan Cen), shiyi@im.ac.cn (Yi Shi).

[†]These authors made equal contributions to this work.

Running title: Inhibition of EBOV infection by berbamine hydrochloride

Abstract Ebola virus (EBOV) infection leads to staggeringly high mortality rate. Effective and low-cost treatments are urgently needed to control frequent EBOV outbreaks in Africa. In this study, we report that a natural compound called berbamine hydrochloride strongly inhibits EBOV replication *in vitro* and *in vivo*. Our work further showed that berbamine hydrochloride acts by directly binding to the cleaved EBOV glycoprotein (GPcl), disrupting GPcl interaction with viral receptor Niemann-Pick C1, thus blocking the fusion of viral and cellular membranes. Our data support the probability of developing anti-EBOV small molecule drugs by targeting viral GPcl. More importantly, since berbamine hydrochloride has been used in clinic to treat leukopenia, it holds great promise of being quickly repurposed as an anti-EBOV drug.

KEY WORDS Ebola virus; Drug repositioning; Entry inhibitor; Primed glycoprotein; Structure-based virtual screening; Protein–protein interaction; Berbamine hydrochloride; Natural compound

1. Introduction

Ebola virus (EBOV) and Marburg virus (MARV) are highly pathogenic. Both viruses belong to the family Filoviridae, and cause acute hemorrhagic fever in humans with high fatality rates[1]. The recent EBOV outbreak (2014–2016) in West Africa claimed over 11,000 lives. However, there is currently no licensed small-molecule drug to treat or prevent EBOV infection, making EBOV a severe public health threat with the possibility of causing a global pandemic[2]. EBOV is a negative-sense enveloped RNA virus. The virus particle is decorated with glycoprotein (GP)[3], which is solely responsible for virus entry[4-6]. GP exists as a trimer, and each monomer consists of two subunits, GP1 and GP2. Following internalization at the cell surface, EBOV transports to the late endosomes where the glycan cap sheathing the receptor-binding region of GP1 is removed by endosomal cathepsin[7]. Thus, primed GP (cleaved GP, GPcl) interacts with the endosomal protein Niemann-Pick C1 (NPC1) and triggers the fusion of viral and endosomal membranes[8-11]. Given the crucial role of GP in viral entry, it has become a primary target for the development of anti-EBOV therapies[12-14].

Indeed, a number of small molecule compounds have been tested for inhibition of EBOV[12,15-18]. Three nucleotide analogues galidesivir (BCX4430)[19,20], remdesivir (GS-5734)[21], and favipiravir (T-705)[22,23], that target RNA synthesis machinery, have been evaluated in clinical trials of Ebola virus disease. However, due to the high mortality or rapid metabolism, further randomized controlled trails are warranted to comprehend the efficacy[24]. Other inhibitors such as MLS000078751, MLS000394177[25], and sunitinib/erlotinib[26] were reported to inhibit the attachment, macropinocytosis, and endolysosome maturation, respectively. Cathepsin inhibitors such as E-64[27,28] and AMS36[29] prevent GP from being cleaved into its fusion-active form. NPC1 binding and fusion can be inhibited by compounds such as compound 3.47, U18666A, MBX2254, MBX2270, SC198, SC073, and SC816[10,30-33]. Besides, a series of compounds, including toremifene, clomiphene, sertraline, bepridil, imipramine, clomipramine and thioridazine, were reported to inhibits fusion by destabilizing the stability of

GP[34-36]. Although these compounds exhibited *in vitro* or *in vivo* antiviral activity, their therapeutic potential needs further evaluation.

We previously identified small peptides that structurally mimic the GPcl-binding region in NPC1 and specifically inhibit EBOV entry[37]. However, one potential drawback of inhibiting a cellular target is the risk of toxicity, which often deters use of such drugs in the clinic. We now report a small molecule with potent anti-EBOV activity that is able to target the receptor-binding site in GPcl.

2. Materials and methods

2.1. Cell lines, plasmids, and virus

HEK293T (Cat# CRL-11268, ATCC), Vero E6 (Cat# CRL-1586, ATCC), and HeLa (Cat# CCL-2, ATCC) cells were cultured in Dulbecco's modified Eagle's medium (DMEM, Gibco) supplemented with 10% fetal bovine serum (FBS, Gibco), 2 mmol/L L-glutamine (Gibco), 50 U/mL penicillin, and 50 ug/mL streptomycin (Macgene) at 37 °C in a humidified atmosphere of 5% CO_2.

Plasmids encoding EBOV-GP, vesicular stomatitis virus envelope protein (VSV-G) and human immunodeficiency virus type 1 (HIV-l) luciferase reporter vector pNL4-3.Luc.R-E- were kept in the Institute of Medicinal Biotechnology, Beijing, China. The GP genes of MARV (GenBank Accession No. ABA87127.1, amino acid [a.a.] 5941–7986) were synthesized by Suzhou GENEWIZ Biotechnology Co., Ltd. (Suzhou, China), and inserted into pcDNA3.1(+) vector (Invitrogen, Shanghai, China). Plasmid encoding *β*-lactamase-Vpr (BlaM-Vpr) was kindly provided by Dr. Xu Tan (Tsinghua University, Beijing, China).

All work with recombinant EBOV expressing enhanced green fluorescent protein (EGFP) (EBOV H.Sapiens-rec/GIN/2014/Makona-Guekedou-C07-EGFP), mouse-adapted EBOV variant Mayinga[38] and wild type MARV variant Angola (MARV H.spaiens-tc/AGO/2005/Angola) was performed in the containment level 4 laboratories at the Canadian Science Centre for Human and Animal Health (CSCHAH), Public Health Agency of Canada, Winnipeg, MB, Canada.

2.2. Compounds and antibodies

TargetMol's small compound library subsets (anti-virus compound library, anti-infection compound library, nature compound library, plant-sourced compound library,

anti-inflammation library, and inhibitors library) were used for virtual screening. Small molecules selected from docking procedure were purchased from Topscience Co., Ltd. (Shanghai, China). Tetrandrine (TET) and efavirenz (EFV) were maintained in the Institute of Medicinal Biotechnology, Beijing, China. The purity of all tested compounds is more than 95%. The following antibodies were used: mouse anti-HIS (TA-02, ZSGB-Bio), mouse anti-FLAG (8146S, CST), rabbit anti-FLAG (B1020, Biodragon), mouse anti-NPC1 (ab134113, Abcam), mouse anti-P24 (ab9071, Abcam), rabbit anti-P24 (produced by our own lab), mouse anti-LAMP1 (ab24170, Abcam), mouse anti-*β*-actin monoclonal antibody (ab6276, Abcam), goat anti-rabbit secondary antibody (ZB-2301, Beijing zhongshan jinqiao Biotechnology), and goat anti-mouse secondary antibody (ZB-2305, Beijing Zhongshan Jinqiao Biotechnology). Alexa Fluor-conjugated secondary antibodies were purchased from Life Technologies.

2.3. Infection assay

Ebola pseudotyped viruses (EBOV-GP/HIV-luc) were produced as previously described[37]. Pseudotyped viruses bearing VSV envelope protein (VSV-G/HIV-luc) and MARV envelope protein (MARV-GP/HIV-luc) were produced in a similar way. The replication-restricted pseudoviruses bearing viral glycoprotein proteins represent a safe method that has been widely used to study the entry of highly infectious viruses[39,40]. Screening of the selected compounds using pesudotyped virus was performed in 96-well plates as previous described[37]. Briefly, cells were infected with the EBOV-GP/HIV-luc in the presence of compounds at a final concentration of 10 μmol/L. The infected cells were lysed, and the anti-EBOV activity of test compounds was evaluated by measuring the luciferase activities at 48 h post infection (hpi). DMSO and TET were used as negative and positive controls, respectively. The VSV-G/HIV-luc was used as a control to determine the specificity of compounds. The 50% effective concentration (EC_{50}) and 90% effective concentration (EC_{90}) values were calculated by using a four-parameter logistic regression in GraphPad Prism 5.

To analyze the retention of EBOV pseudoparticle (EBOVpp) virions in newly infected cells, HEK293T cells were infected with EBOV-GP/HIV-luc at multiplicity of infection (MOI) of 1.0 in the presence of MG132 (4 μmol/L). After 4 h, cells were fixed in 4% paraformaldehyde for 30 min on ice and virus was stained with rabbit or mouse anti-p24 antibody, followed by an anti-rabbit AlexaFluor-555 antibody or anti-mouse AlexaFluor-488

antibody. Fluorescence was monitored with a confocal microscope (PerkinElmer UltraVIEW VoX, Germany) with a 100× oil objective lens.

To assess the effect of berbamine hydrochloride on EBOV and MARV replication, Vero E6 cells were pretreated with drug (0 to 200 μmol/L) or DMSO for 1 h at 37 °C and infected at a MOI of 0.1 with EBOV expressing EGFP (EBOV-EGFP) or wild type MARV for 1 h at 37 °C, after which the inoculum was removed and replaced with fresh medium (DMEM plus 2% FBS). Cells were further incubated for 72 h in the presence of EEI-10 or DMSO. For EBOV-EGFP-infected cells fluorescence was quantified on a Synergy HTX plate reader (BioTek, Winooski, VT, USA). The percent relative infectivity was determined by comparing fluorescence readings of EEI-10 treated cells to those of DMSO treated control cells. For MARV infected cells, supernatants were harvested, and viral RNA was quantified, as described below. The percent relative infectivity was determined by comparing the amount of viral RNA detected in EEI-10 treated cells to that of DMSO treated control cells.

2.4. Real-time quantitative PCR (qRT-PCR)

For HIV-based infections, total RNA was extracted from infected cells by use of an RNA extraction kit (Tiandz, Beijing, China). The level of viral RNA was determined by performing qRT-PCR analysis by use of a one-step SYBR PrimeScript RT-PCR kit (TaKaRa, Dalian, China). The primer pair (5′-TTAAGCCTCAATAAAGCTTGCC-3′ and 5′-GTTCGGGCGCCACTGCTAGA-3′) amplifies the long-terminal repeats of HIV. Levels of cellular glyceraldehyde-3-phosphate dehydrogenase (GAPDH) RNA were amplified with primers 5′-ATCATCCCTGCCTCTACTGG-3′ and 5′-GTCAGGTCCACCACTGACAC-3′; the results served as an internal control to normalize the level of HIV RNA.

For MARV infections, viral RNA was extracted from cell culture supernatants using the QIAamp viral RNA mini kit (Qiagen, Hilden, Germany). Viral RNA levels were quantified by qRT-PCR using the LightCycler 480 thermal cycler (Roche, Germany) and the LightCycler 480 RNA Master Hydrolysis Probes kit (Roche, Germany) along with the following primers and probe:

1-F, 5′-GCAAAAGCATTCCCTAGTAACATGA-3′;

1-R, 5′-CACCCCTCACTATRGCGTTYTC-3′;

2-F, 5′-GCGAAGGCATTCCCTAGTAATATGA-3′;

2-R, 5′-CACCTCTTACTATGGCATTCTC-3′;

probe, 5′-56-FAM/TGGCACCAY/ZEN/AATTCAGCAAGCATAGG/3IABkFQ-3′.

Cycling conditions were as follows: 63 °C for 3 min and 95 °C for 30 s, then 45 cycles of 95 °C for 15 s and 60 °C for 30 s.

2.5. Cytotoxicity analysis

HEK293T and Vero E6 cells were seeded in 96-well plates. Following overnight incubation at 37 °C, TET and berbamine hydrochloride were added at different concentrations used for the viral infection studies. Cells in culture media without drug served as control. At 48 h, cell counting kit-8 (CCK-8, Beyotime, Shanghai, China) was used to evaluate cell viability.

2.6. BlaM-Vpr releasing assay

For production of pseudotyped viruses incorporating BlaM-Vpr, HEK293T cells were transfected with 6 μg of pNL4-3.Luc.R-E-, 6 μg of pEbola-GP or pVSV-GP, 3 μg of pBlaM-Vpr and 1.5 μg of pAdvantage using Lipo2000 in 10-cm dishes. Culture supernatants were collected after 48 h and filtered through a 0.45 μm filter. The virus was concentrated by ultracentrifugation at 138,900 × *g* for 4 h pelleting through a 20% sucrose cushion or by 100 kDa molecular weight cutoff centrifugal filters. Detection of virus capsid release into the cell cytoplasm was performed using LiveBLAzer FRET-B/G Loading Kit with CCF4-AM (Invitrogen) according to manufacturer instructions. Briefly, HeLa or SupT1 cells were seeded on 6-well plates 1 day before the assay. After preincubation with each drug for 1 h, cells were infected with EBOV-GP/HIV-luc or VSV-GP/HIV-luc for 2 h at 37 °C in the presence of the drug. After loading CCF4-AM substrate, cells were fixed in 4% paraformaldehyde. Amcyan or Pacific Blue fluorescence signals were detected by fluorescence-activated cell sorting (FACS) method.

2.7. Time-of-addition experiment

Berbamine hydrochloride (1 μmol/L), TET (1 μmol/L) and EFV (5 nmol/L) were added to the 293T cell culture medium before infection (–1 h), during infection (0 h), and 1, 4, 5, 6, 8, 18, and 24 hpi. Viral replication was determined at 48 hpi as described above. Cell culture treated with DMSO or TET was used as negative and positive control, respectively. The HIV-1 reverse transcriptase inhibitor EFV was used to confirm the rationality of our assay system.

2.8. Virus binding experiment

For binding tests, 4×10^5 HEK293T cells were seeded in 6-well plates overnight and infected with EBOV-GP/HIV-luc for 1 h at 4 ℃ in the presence of TET (5 μmol/L), berbamine hydrochloride (5 μmol/L) and heparin (5 μg/mL), followed by washing with PBS, and virus absorption on the cell surface was quantified through the measurement of viral genomic RNA by qRT-PCR.

2.9. In vitro protease cleavage of EBOV-GP/HIV-luc

Concentrated EBOV-GP/HIV-luc was stocked in HEPES-MES buffer (40 mmol/L HEPES, 40 mmol/L morpholinepropanesulfonic acid, 50 mmol/L NaCl, 0.5mmol/L $CaCl_2$, pH 7.5), the GP protein was cleaved by 0.5 mg/mL thermolysin (Promega, Madison, WI, USA) at 37 °C for 1 h. The reaction was stopped by 0.5 mmol/L EDTA and protease inhibitors. The cleavage efficiencies were confirmed by immunoblotting using anti-FLAG antibody. Then HEK293T cells were incubated with the cleaved or uncleaved EBOV-GP/HIV-luc in the presence of the drug for 48 h, the luciferase activities were detected to evaluate the antiviral efficiencies of drugs.

2.10. In situ proximity ligation assay (PLA)

In situ PLA was performed using Duolink PLA starter kits (DUO92101, Sigma–Aldrich) according to the manufacturer. Briefly, 4% paraformaldehyde-fixed samples were incubated with blocking solution to saturate nonspecific binding and subsequently with primary antibodies at 37 °C for 1 h. Thereafter, slides were incubated for 1 h at 37 °C with Duolink PLA probes. Ligation solution was added for 30 min at 37 °C. Ligation solution was removed with wash buffer A, and amplification solution was added for 100 min at 37 ℃ and removed with wash buffer B. Finally, Duolink *in situ* mounting medium with 4′,6-diamidino-2-phenylin-dole (DAPI) was added. Fluorescence was monitored with a confocal microscope (PerkinElmer UltraVIEW VoX, Germany) with a 100 × oil objective lens.

2.11. Protein production and purification

The NPC1-C (residues 374 to 620) gene and the corresponding mutant (F503AF504AY506) gene were cloned into pGEX-4T-1 vector. All plasmids were transformed into *E. coli* BL21

(DE3) and cultured in Luria–Bertani (LB) medium containing 100 mg/L ampicillin at 37 °C when OD600 reached 0.6–0.8. Protein was induced with 0.5 mmol/L isopropyl *β*-D-1-thiogalactopyranoside (IPTG) for more than 18 h at 16 °C. Bacterial cells were collected by centrifugations at 7000 rpm (3-18K, Sigma, Osterode am Harz, Germany) for 20 min and resuspended in a buffer (25 mmol/L HEPES, pH 7.4, 150 mmol/L NaCl, 1 mmol/L dithiothreitol (DTT)). Resuspended cells were lysed by sonication and cell debris were removed by centrifugation at 10,000 rpm (3-18K, Sigma, Osterode am Harz, Germany) for 10 min. Cell supernatants were subjected to a GSTrap^{TM} column (GE Healthcare, USA) for initial purification. The target proteins were obtained in elution buffer (25 mmol/L HEPES, pH 7.4, 150 mmol/L NaCl, 1 mmol/L DTT, 10 mmol/L reduced glytathione). Fractions were pooled and loaded onto a Superdex 200 10/300 Increase column (GE Healthcare, USA) in a buffer (25 mmol/L HEPES, pH 7.4, 150 mmol/L NaCl, 1 mmol/L DTT). The final product was concentrated to 4 mg/mL and stored at –80 °C before use.

2.12. The glutathione S-transferase (GST) pull-down assay

Briefly, 10 μg GST-NPC1-C protein (or its mutants) and 10 μg GPcl-HIS were mixed with glutathione beads (Beyotime, BeyoGoldTM GST-tag purification resin) in reaction buffer (25 mmol/L HEPES, pH 7.4, 150 mmol/L NaCl) for 2 h at 4 ℃ on a rotating platform. For drug blocking test, 10 μg GPcl-HIS was primarily mixed with EEI-10 or TET for 1 h at 4 ℃ before adding 10 μg GST-NPC1-C protein (or its mutants) and glutathione beads, and the mixtures were incubated at 4 ℃ for another 2 h. Then washes beads with reaction buffer for three times, beads bound with proteins were mixed with 50 μL 1×SDS loading buffer and heated for 10 min at 100 ℃. After centrifugation, these samples were measured by Western blotting using anti-GST and anti-HIS antibodies.

2.13. Co-immunoprecipitation (co-IP) for Ebola GPcl and NPC1

HEK293T cells were transfected with plasmid expressing NPC1-C-FLAG using Lipo2000 in 10 cm dishes for 48 h, cells were lysed by NP40 and debris was removed through centrifugation at 12,000 rpm (Pico 17, ThermoFisher, Osterode am Harz, Germany) for 10 min. TET (10 μmol/L), berbamine hydrochloride (10 μmol/L) were pre-incubated with GPcl-HIS (1 μg) for 1 h before mixing with cell lysate. Anti-HIS antibody coated beads were used to pull down GPcl-HIS and the bound NPC1-C-FLAG was detected through Western blotting.

2.14. Analysis of intracellular cholesterol

Hela cells were pretreated with TET (5 μmol/L), berbamine hydrochloride (5 μmol/L), U18666A (5 μmol/L) for 24 h, and then cells were collected and fixed with paraformaldehyde (4%) for 30 min on ice. After three PBS washes, cells were incubated with 50 μg/mL filipin III complex in the dark for 1 h at room temperature. After three PBS washes, cells were detected by FACS in the DAPI channel.

2.15. Bio-layer interferometry (BLI) binding assay

Octet RED96 (ForteBio/Pall Life Sciences, Menlo Park, CA, USA) was used to measure binding affinity and kinetic profile. The purified GPcl was biotinylated by EZ-Link NHS-LC-LC-Biotin (Thermo Scientific). The biotinylated GPcl (50 μg/mL) was then captured *via* super streptavidin (SSA) biosensors (120 s, at 30 °C, with a stirring speed of 1000 rpm [Octet RED96]). A duplicate set of sensors were incubated in assay buffer (0.002% Tween-20, PBS, pH=7.4) without protein for use as a background binding control. Both the ligand and reference biosensors were quenched with 5 μg/mL biotin for 1 min. For binding affinity constant K_D (K_D=k_{dis}/k_{on}) determination, the binding of a dilution series of compounds was detected for 60 s association (k_{on}, L/mol·s) followed by 60 s dissociation (k_{dis}, 1/s) in parallel to the ligand biosensors and reference biosensors. Besides, blank binding cycles using buffer only were used to correct the baseline shift during the analysis. After measurements were complete, a double reference subtraction method was processed to subtract the effect of baseline drift and nonspecific binding. K_D acquired from fitting into 1:1 binding model by global fitting of multiple kinetic traces and analyzed by Data Analysis 9.0 software.

2.16. Pharmacokinetics

Female ICR mice were orally administered 25 mg/kg EEI-10, after which plasma was collected *via* orbital puncture at 8 timepoints (15, 30 min, 1, 2, 4, 6, 8, and 24 h) in tubes containing EDTA-K2 followed by plasma separation by centrifugation at 5000 rpm (IKA-VIBRAX VXR, IKALabortechnik, Staufen, Germany) for 10 min at 4 °C. Plasma samples were stored at –80 °C for further processing and analysis. 10 μL of plasma samples were placed into a 1.5 mL Eppendorf tube. After the addition of 100 μL internal standard (60.0 ng/mL dexamethasone), the samples were vortex mixing for 60 s, and then centrifuged at 12,000 rpm (IKA-VIBRAX VXR, IKALabortechnik, Staufen, Germany) for 3 min. The supernatant was

then transferred into 96-well plates, and 10 μL aliquot was injected into the LC–MS/MS system for analysis. Pharmacokinetics data analysis was performed using WinNonlin Professional v6.3 (Pharsight, USA) by a non-compartmental analysis method to obtain pharmacokinetic parameters.

2.17. Computational methods

Using Auto-Dock Vina package[41], structure-based virtual screening was carried out over 4114 compounds in the focused database. Based on the crystal structure of GPcl in complex with the receptor, we first generated the docking parameter files using AutoDockTools-1.5.6. The grid center was located at the receptor-binding region on the head of GPcl and was designated at dimensions (*x*, *y*, and *z*): 34.428 Å, –17.200 Å, and –317.00 Å. The grid size was set to 24 Å, 28 Å, and 28 Å on *X*, *Y* and *Z* coordinates, respectively. Then we used Open Babel software to create the ligand parameter files for docking[42]. Each compound in the library was assigned hydrogen at pH 7.4 and converted to PDBQT format. Finally, all these compounds were docked to GPcl and ranked by their calculated binding free energies (ΔG_{ADV}). The molecular dynamic simulation and molecular mechanics generalized born surface area (MM/GBSA) calculation were performed as previously described[37,43].

2.18. Animal ethics statement

Animal experiments were performed in the containment level 4 laboratories at CSCHAH. All experimental protocols were reviewed and approved by the institutional animal care committee in accordance with guidelines from the Canadian Council on Animal Care. All staff working on animal experiments completed education and training programs according to the standard protocols appropriate for this level of biosafety.

2.19. Efficacy of berbamine hydrochloride in EBOV-infected mice

Six- to eight-week-old female BALB/c mice (Charles River) were inoculated intraperitoneally with the 1000 × 50% lethal dose (LD_{50}) of MA-EBOV. Mice were treated with 100 mg/kg of body weight of berbamine hydrochloride *via* oral administration beginning on either day –1 or day +1 post-infection and continuing daily up to day 6 post-infection. Animals in the control group were treated with PBS following the same schedule. Mice were observed daily for weight change and clinical signs.

2.20. Statistical analysis

Data are presented as mean ± standard deviation (SD) from at least three independent experiments. Statistical comparisons of the Kaplan–Meier survival curves (Fig. 6B and D) were performed using the Log-rank test. *P*-values are indicated as follows: $*P \leq 0.05$, $**P \leq 0.01$, $***P \leq 0.001$, n.s. represents not significant.

3. Results

2.1. Identification of berbamine hydrochloride as an EBOV entry inhibitor

We previously characterized the NPC1-binding site in GPcl, consisting of residues V79, T83, K84, F88, I113, V141, and P146[37] (Fig. 1A). Based on this result, we designed a virtual screening strategy, as shown in Fig.1B, and systematically examined 4114 compounds from the focused small compound libraries, and ranked these compounds based on the predicted binding free energies (ΔG_{ADV}) (Supporting Information Fig. S1). A total of 334 compounds had a ΔG_{ADV} lower than –9.0 kcal/mol and were further visually inspected for H-bond, π–π, or salt bridge interactions to discard unrealistic poses with unreasonably high score. A final list of 46 compounds (Supporting Information Table S1) were selected for further study.

We first assessed the inhibitory effect of the selected 46 compounds on infection of HIV-Luc reporter virus that was pseudotyped with EBOV GP (EBOV pseudoparticle, EBOVpp) or VSV GP (VSV pseudoparticle, VSVpp), as we described previously[37]. Of these 46 compounds, EEI-10 (Fig. 1C), EEI-33 and EEI-45 (Supporting Information Fig. S2) exhibited more than 80% inhibition of EBOVpp infection, but less than 20% reduction in VSVpp infectivity, suggesting that the three compounds selectively block EBOV GP-mediated viral entry. Such a selective inhibition was also observed for the known EBOV entry inhibitor tetrandrine (thereafter called TET)[44]. Next, we determined the binding affinity of the selected compounds to the purified GPcl *in vitro* in the BLI binding assay. The association and dissociation data suggest that only EEI-10 and EEI-20 interacted directly with GPcl with a K_D of 217 and 229 μmol/L, respectively (Fig. 1D and Supporting Information Fig. S3). Together, among the 46 compounds tested, only EEI-10 both binds to GPcl and selectively inhibits EBOV GP-mediated viral entry. Furthermore, we investigated if EEI-10 is able to compete with NPC1 *in vitro* for binding to GPcl in a GST pull-down assay using the recombinant protein GST-NPC1-C (C-terminus of NPC1 fused with GST) and GPcl

(Supporting Information Fig. S4). A significant reduction is found in bound GPcl by EEI-10 in a dose dependent fashion (Fig. 1E and F). This suggests that EEI-10 may inhibit fusion of viral and endosomal membranes by blocking the binding of GPcl to NPC1, resulting in the inhibition of EBOV GP-mediated viral entry.

EEI-10, also called berbamine hydrochloride, is a natural compound extracted from the berberis amurensis and has been used in the clinic to treat leukopenia[45]. Repurposing of an approved drug to inhibit EBOV represents a great opportunity of developing new anti-EBOV drugs. We thus decided to further characterize EEI-10 inhibition of EBOV. First, we observed that EEI-10 profoundly inhibited EBOVpp but not VSVpp (Fig. 1G). Results of dose–response experiments revealed a concentration-dependent inhibition of EBOVpp in 293T cells with EC_{50} of 0.49 μmol/L (EC_{90} =2.10 μmol/L) (Fig. 1H). No cytotoxic effect of EEI-10 was observed even at 10 μmol/L (Supporting Information Fig. S5A). Importantly, EEI-10 potently suppressed EBOV infection of Vero E6 cells (EC_{50} = 4.1 ± 1.06 μmol/L, EC_{90} =7.6 μmol/L) (Fig. 1I and Supporting Information Table S2) and did not affect cell viability at the concentrations used (Fig. S5B). These data together suggest that EEI-10 is a potent EBOV inhibitor.

Insert Fig. 1

2.2. EEI-10 inhibits EBOV GP-mediated fusion of viral and cellular membranes

The *in vitro* data support that EEI-10 suppresses EBOV infection by inhibiting fusion of viral and endosomal membranes (Fig. 1). To further validate the idea, we first performed a time-of-addition experiment using EBOVpp. EEI-10 was added at different time points before and after EBOVpp infection. The results showed that both EEI-10 and TET markedly inhibited viral infection at the early time points of drug addition, and their inhibitory effects decreased after 4 hpi (Fig. 2A). In contrast, the HIV-1 reverse transcriptase inhibitor efavirenz (EFV) maintained its inhibitory effect up to 8 hpi. We further measured the possible effect of EEI-10 on the internalization of EBOVpp from the cell surface by quantifying the uptake of viral genomic RNA, and observed no effect as opposed to the marked inhibition by heparin (Fig. 2B), which has been shown to block the early attachment of EBOV to the target cells[46]. These data support that EEI-10 inhibits an early step of EBOVpp infection, after EBOV GP-mediated internalization from the cell surface but prior to viral RNA replication.

It is known that following internalization at the cell surface, EBOV particles translocate to the acidic late endosomes where virus-cell membrane fusion occurs, leading to the release of viral RNA into the cytoplasm[47,48]. Imaging EBOVpp-infected cell at 4 hpi revealed a similar number of virions in the LAMP1-positive late endosome/lysosome compartments in cells treated with either EEI-10 or control DMSO (Fig. 2C and Supporting Information Fig. S6). This further supports the data in Fig. 2B that EEI-10 does not affect the early events of virus entry from uptake of virus at the cell surface to trafficking of virions to the acidic compartments. We next tested whether the fusion of viral and cellular membranes is inhibited by EEI-10 using a BlaM-Vpr release assay that has been established to measure the delivery of HIV-1 core into the cytoplasm[49]. We found that EEI-10 significantly reduced the cytoplasmic entry of BlaM-Vpr from EBOVpp by approximate 80%, whereas no such effect of EEI-10 was observed for VSVpp (Fig. 2D and Supporting Information Fig. S7). This suggests that EEI-10 specifically inhibits the delivery of BlaM-Vpr into the cytoplasm resulting from EBOV GP-mediated membrane fusion. In further support of this conclusion, adding the proteasome inhibitor MG132[50] to cell culture for preventing the degradation of incoming virion, a pronounced increase was detected in the level of EBOVpp particles in newly infected cells treated with either EEI-10 or TET, but not for VSVpp infection (Fig. 2E and Supporting Information Fig. S8), suggesting that EEI-10-mediated delay of virus entry at the late endosomes causes accumulation of EBOVpp particles.

Insert Fig. 2

2.3. EEI-10 disrupts binding of EBOV GPcl to NPC1

We next determined whether EEI-10 inhibits EBOV GP-mediated entry by disrupting the binding of GPcl to its receptor NPC1 in the infected cell. We first observed that that EEI-10 treatment reduced the colocalization of EBOVpp particles with NPC1 in the infected cells (Fig. 3A), as opposed to TET which targets the two-pore channels and had no effect as previously reported[44]. EBOV GP can only bind to NPC1 after cleavage by the endosomal cathepsin. We thus pretreated EBOVpp with the protease thermolysin, which completes GP cleavage[8], and then infected cells in the presence of EEI-10. Again, strong inhibition was observed with EEI-10 but not with cysteine protease inhibitor E-64[27,28] (Fig. 3B). Thus, EEI-10 diminishes the colocalization of EBOVpp with NPC1 not through affecting GP proteolysis. We next performed co-immunoprecipitation to measure the association of GPcl

with its receptor NPC1 and found that EEI-10, but not TET, markedly reduced GPcl-NPC1 interaction (Fig. 3C). This observation was supported by the data of PLA, showing that treatment with EEI-10 diminished GPcl-NPC1 interaction in the infected cells by approximately 80% (Fig. 3D). We further showed that EEI-10 did not affect the cellular content of cholesterol (Supporting Information Fig. S9) in contrast with NPC1 inhibitors U18666A[30] and compound 3.47[10] that inhibited EBOV entry by causing cholesterol accumulation in late endosomes, suggesting that EEI-10 does not act on NPC1. Together with the *in vitro* data (Fig. 1), we thus conclude that EEI-10 binds to GPcl, prevents GPcl from binding NPC1, and inhibits GP-mediated fusion of viral and cellular membranes.

Insert Fig. 3

2.4. GPs of EBOV and MARV share a similar binding pocket for EEI-10 and are both inhibited by EEI-10

We next used the AutoDock Vina computation program to model the binding of EEI-10 to GPcl. In the generated model of GPcl in complex with EEI-10 (Fig. 4A), EEI-10 is located at the hydrophobic pocket in GPcl and forms hydrogen bond interaction with the amino residue E112. We further employed MM/GBSA computation approach to calculate the binding free energy of EEI-10 and decomposed the free energy at the amino acid level. The cavity analysis showed that the major contributing amino acids to the binding of EEI-10 include E112, T83, I113, V141, F88, L111, W86, V79, P80, and G143, which are ranked based on their ΔG_{ADV} in the range from –2.54 to –0.62 kcal/mol (Supporting Information Table S3).

To validate this binding model, we mutated the three top-ranking amino acids E112, T83 and I113, and examined their effect on the sensitivity of EBOV GP-mediated entry to EEI-10. The E112A mutation severely impaired viral infectivity, thus was not further tested for EEI-10 inhibition (Supporting Information Fig. S10). The I113A GP mutant was refractory to EEI-10 while remaining sensitive to the TET entry inhibitor (Fig. 4B). In the meantime, the T83A mutation exerted no effect on the sensitivity of GP to either EEI-10 or TET inhibition (Fig. 4B); this is likely because A83 is able to restore the van der Waals interaction with EEI-10 which is observed for T83 as predicted in our computation model (Table S3). These data demonstrate that I113 is a key residue in contact with EEI-10 and that its mutation leads to resistance to EEI-10, which supports the structural model of GPcl binding to EEI-10.

Recent studies have revealed a common receptor-binding site in GPs of several filoviruses including EBOV and MARV[14,51,52], suggesting that EEI-10 may inhibit MARV infection as well. Indeed, EEI-10 inhibited the MARV-GP/HIV-luc virus infection at an EC_{50} = 0.99 μmol/L, and inhibited MARV itself at an EC_{50} = 4.06 ± 3.03 μmol/L (Fig. 4C, D and Table S2). We further conducted computational docking of EEI-10 to MARV-GP1 and then preformed molecular dynamic simulation to relax the complex. The binding free energy of the MARV GP/EEI-10 was calculated as ΔG_{ADV} = –9.3 kcal/mol, which is moderately higher than that of EBOV–GPcl/EEI-10 complex (ΔG_{ADV} = –10.9 kcal/mol). Notably, these two complexes are well superposed at the EEI-10 binding sites (Fig. 4E). The top 10 amino acids in MARV-GP1 that contribute most to the binding energies are L64, S67, K68, A71, F72, I95, V97, I125, G127, and N129 (Supporting Information Table S4), which are equivalent to P80, T83, K84, G87, F88, L111, I113, V141, G143, and G145 in EBOV GPcl. Importantly, seven of the top 10 major contributing amino residues are shared in both complexes (Fig. 4F). These data suggest that EEI-10 is able to bind to the GPs of EBOV and MARV, and inhibits both viruses.

Insert Fig. 4

2.5. EEI-10 protects mice from lethal EBOV infection

Finally, we asked whether EEI-10 was able to protect mice from lethal EBOV infection. Assessment of EEI-10 plasma pharmacokinetics (PK) parameters in the ICR female mice revealed that EEI-10 exhibited a low level of oral bioavailability (Fig. 5 and Supporting Information Table S5). Following a single 25 mg/kg oral doses of EEI-10, the maximum concentration (C_{max}) and daily systemic exposure ($AUC_{0–24\,h}$) of EEI-10 was 1.03 μmol/L and 12.5 μmol/L·h, respectively. Considering that EEI-10 had a low order of acute toxicity in mice, with the LD_{50} value of 1.7 ± 0.2 g/kg[53], mice were treated orally once per day for 6 days with 100 mg/kg EEI-10 beginning the day prior to inoculation with a lethal dose of mouse-adapted EBOV (MA-EBOV) (Fig. 6A). Remarkably, 100% of the mice treated with EEI-10 survived infection while only one of the PBS-treated animals survived (Fig. 6B), although all exhibited weight loss (Fig. 6C). To determine whether EEI-10 was also effective if treatment was begun post-infection, mice were again inoculated with MA-EBOV and then treated orally with the same dose of drug beginning on the 1st day post-infection for a period of 6 days. Whereas all PBS-treated mice succumbed to infection by Day 7, nearly all mice treated with EEI-10 survived, and the time to death was prolonged in the single treated animal

that died (Fig. 6D). Again, all animals exhibited weight loss (Fig. 6E), suggesting that, while EEI-10 treatment provided a significant survival advantage, it did not prevent some signs of disease.

Insert Fig. 6

4. Discussion

This remarkable protective efficacy of EEI-10 may be partially attributed to the relatively weak interaction of GPcl with its receptor NPC1. With a K_D of 158 μmol/L, as measured *in vitro* using recombinant proteins[11], the interaction between these two proteins was likely easily disrupted by EEI-10. Given that EEI-10 is directly targeting EBOV GPcl rather than a host factor, there exists the problem of virus escape mutations. Our data demonstrated that I113 is a key residue in contact with EEI-10 and that its mutation leads to resistance to EEI-10. It has been reported that I113A have a defect in virion incorporation[6], and thus may generate a genetic barrier to resistance development. Besides, through medicinal chemistry to modify EEI-10 and select for variants with greater affinity to GPcl, we expect to identify EEI-10 derivatives exhibiting much stronger inhibition of EBOV as well as a higher genetic barrier to deter the development of viral resistance. Additionally, as a drug to treat leukopenia, EEI-10 is expected to modulate certain cellular pathways and host immunity, which may have also contributed to its protection of mice against lethal EBOV infection.

Of note, EEI-10 was demonstrated to bind to EBOV GPcl and potently inhibit virus entry, whereas *in vitro* binding assay revealed that EEI-10 exhibited a low affinity for GPcl, with K_D values above 100 μmol/L (Fig. 1D), which is much higher than its EC_{50} in micromolar range for inhibition of viral infection. Similarly, we observed the discrepancy between the concentration of EEI-10 to inhibit the interaction between GPcl and NPC1 *in vitro* (50 μmol/L for 50% inhibition) and in cell (10 μmol/L for more than 80%) (Figs. 1 and 3). This raises the possibility of enhanced potency of EEI-10 in physiological condition through either enhanced binding of GPcl or additional effect upon membrane fusion. Although the detail mechanism awaits further investigation, the observation that mutated residue in contact with EEI-10 leads to resistance to the compound supports that the antiviral activity largely depends on its binding of EBOV GPcl.

Virtual screening method has proven efficient in accelerating drug discovery for its knowledge-driven, cost-benefit and time-saving advantages. Since the three-dimensional

structure of target protein is available, we applied structure-based virtual screening of commercial chemical databases against the receptor binding site of EBOV GPcl. Using this technique, we have identified a natural compound berbamine hydrochloride (EEI-10) that potently inhibits EBOV infection of cultured cells through direct binding to viral GPcl and impairing the interaction of GPcl with the viral receptor NPC1. Our data further showed that EEI-10 strongly inhibits another pathogenic filovirus, MARV, implicating the potential use of EEI-10 as a broad-spectrum inhibitor of filovirus infection, while further studies on other strains of filovirus are warranted to comprehend the efficacy.

5. Conclusions

Overall, starting from the structure-based virtual screening, we identified a natural compound berbamine hydrochloride (EEI-10) that strongly inhibits EBOV replication *in vitro* and *in vivo*. This compound binds to the EBOV–GPcl, disrupts the interaction between GPcl and viral receptor NPC1, and thus blocks the fusion of viral and cellular membranes. These findings further support the feasibility of inhibiting EBOV entry by targeting GPcl with small molecules. Given that berbamine hydrochloride is already approved to treat leukopenia and has been thoroughly evaluated for its safety and pharmacokinetics properties, this drug holds great promise for saving the lives of EBOV patients and preventing future EBOV epidemics or pandemics.

Acknowledgments

We thank Public Health Agency of Canada for the assistance in evaluation the effects of compound on EBOV and MARV infection. This research was funded by the CAMS Innovation Fund for Medical Sciences (Grant Nos. 2021-I2M-1-030 and CAMS-I2M-1-012, China), the National Natural Science Foundation of China (Grant Nos. 81802019, 81902075 and 81673358), the National Mega-project for Innovative Drugs (Grant No. 2018ZX09711003-002-002, China), the Beijing Natural Science Foundation (Grant No. 7184228, China), the Peking Union Medical College Youth Fund (Grant Nos. 3332016063 and 3332018096, China), the China Ministry of Science and Technology National 973 Project (Grant No. 2014CB542503), the Excellent Young Scientist Program from the NSFC (Grant No. 81622031, China), and the National Key Research and Development program of China (Grant No. 2016YFD0500307).

Author contributions

Dongrong Yi executed all the *in vitro* antiviral testing against pesudotyped virus. Quanjie Li performed the structure-based virtual screening, evaluated the binding kinetics of compounds, and calculated the binding mode of compounds. Han Wang purified the protein samples. Kai Lv and Mingliang Liu coordinated pharmacokinetics studies. Ling Ma and Jing Wang established the EBOVpp entry inhibitor evaluation system. Yujia Wang and Yongxin Zhang conducted cell-based assays for cytotoxicity. Dongrong Yi, Quanjie Li, and Shan Cen wrote the initial draft. Xiaoyu Li, Yi Shi, Jianxun Qi, George F. Gao, and Shan Cen supervised all of the research. All authors participated in the discussion and approved the manuscript.

Conflicts of interest

The authors declare no conflict of interest.

References

1 Feldmann H, Geisbert TW. Ebola haemorrhagic fever. *Lancet* 2011;**377**:849-62.

2 Jacob ST, Crozier I, Fischer WA 2nd, Hewlett A, Kraft CS, Vega MA, et al. Ebola virus disease. *Nat Rev Dis Primers* 2020;**6**:13.

3 Volchkov VE, Volchkova VA, Muhlberger E, Kolesnikova LV, Weik M, Dolnik O, et al. Recovery of infectious Ebola virus from complementary DNA: RNA editing of the GP gene and viral cytotoxicity. *Science* 2001;**291**:1965-9.

4 Chandran K, Sullivan NJ, Felbor U, Whelan SP, Cunningham JM. Endosomal proteolysis of the Ebola virus glycoprotein is necessary for infection. *Science* 2005;**308**:1643-5.

5 Takada A, Robison C, Goto H, Sanchez A, Murti KG, Whitt MA, et al. A system for functional analysis of Ebola virus glycoprotein. *Proc Natl Acad Sci U S A* 1997;**94**:14764-9.

6 Manicassamy B, Wang J, Jiang H, Rong L. Comprehensive analysis of Ebola virus GP1 in viral entry. *J Virol* 2005;**79**:4793-805.

7 Dube D, Brecher MB, Delos SE, Rose SC, Park EW, Schornberg KL, et al. The primed Ebolavirus glycoprotein (19-kilodalton GP1, 2): sequence and residues critical for host cell binding. *J Virol* 2009;**83**:2883-91.

8 Carette JE, Raaben M, Wong AC, Herbert AS, Obernosterer G, Mulherkar N, et al. Ebola virus entry requires the cholesterol transporter Niemann-Pick C1. *Nature* 2011;**477**:340-3.

9 Miller EH, Obernosterer G, Raaben M, Herbert AS, Deffieu MS, Krishnan A, et al. Ebola virus entry requires the host-programmed recognition of an intracellular receptor. *EMBO J* 2012;**31**:1947-60.

10 Côté M, Misasi J, Ren T, Bruchez A, Lee K, Filone CM, et al. Small molecule inhibitors reveal Niemann–Pick C1 is essential for Ebola virus infection. *Nature* 2011;**477**:344-8.

11 Wang H, Shi Y, Song J, Qi J, Lu G, Yan J, et al. Ebola viral glycoprotein bound to its endosomal receptor Niemann-Pick C1. *Cell* 2016;**164**:258-68.

12 Hoenen T, Groseth A, Feldmann H. Therapeutic strategies to target the Ebola virus life cycle. *Nat Rev Microbiol* 2019;**17**:593-606.

13 Misasi J, Sullivan NJ. Immunotherapeutic strategies to target vulnerabilities in the Ebolavirus glycoprotein. *Immunity* 2021;**54**:412-36.

14 Bornholdt ZA, Ndungo E, Fusco ML, Bale S, Flyak AI, Crowe JE, et al. Host-primed Ebola virus GP exposes a hydrophobic NPC1 receptor-binding pocket, revealing a target for broadly neutralizing antibodies. *MBio* 2016;**7**:e02154-15.

15 Mirza MU, Vanmeert M, Ali A, Iman K, Froeyen M, Idrees M. Perspectives towards antiviral drug discovery against Ebola virus. *J Med Virol* 2019;**91**:2029-48.

16 Chakraborty C. Therapeutics development for Ebola virus disease: a recent scenario. *Curr Opin Pharmacol* 2021;**60**:208-15.

17 Morales-Tenorio M, Ginex T, Cuesta-Geijo MÁ, Campillo NE, Muñoz-Fontela C, Alonso C, et al. Potential pharmacological strategies targeting the Niemann-Pick C1 receptor and Ebola virus glycoprotein interaction. *Eur J Med Chem* 2021;**223**:113654.

18 Cheng H, Lear-Rooney CM, Johansen L, Varhegyi E, Chen ZW, Olinger GG, et al. Inhibition of Ebola and Marburg virus entry by G protein-coupled receptor antagonists. *J Virol* 2015;**89**:9932-8.

19 Warren TK, Wells J, Panchal RG, Stuthman KS, Garza NL, Van Tongeren SA, et al. Protection against filovirus diseases by a novel broad-spectrum nucleoside analogue BCX4430. *Nature* 2014;**508**:402-5.

20 Taylor R, Kotian P, Warren T, Panchal R, Bavari S, Julander J, et al. BCX4430—a broad-spectrum antiviral adenosine nucleoside analog under development for the treatment of Ebola virus disease. *J Infect Public Health* 2016;**9**:220-6.

21 Warren TK, Jordan R, Lo MK, Ray AS, Mackman RL, Soloveva V, et al. Therapeutic efficacy of the small molecule GS-5734 against Ebola virus in rhesus monkeys. *Nature* 2016;**531**:381-5.

22 Oestereich L, Ludtke A, Wurr S, Rieger T, Munoz-Fontela C, Gunther S. Successful treatment of advanced Ebola virus infection with T-705 (favipiravir) in a small animal model. *Antiviral Res* 2014;**105**:17-21.

23 Furuta Y, Komeno T, Nakamura T. Favipiravir (T-705), a broad spectrum inhibitor of viral RNA polymerase. *Proc Jpn Acad Ser B Phys Biol Sci* 2017;**93**:449-63.

24 Mulangu S, Dodd LE, Davey RT Jr, Tshiani Mbaya O, Proschan M, Mukadi D, et al. A randomized, controlled trial of Ebola virus disease therapeutics. *N Engl J Med* 2019;**381**:2293-303.

25 Anantpadma M, Kouznetsova J, Wang H, Huang R, Kolokoltsov A, Guha R, et al. Large-scale screening and identification of novel Ebola virus and Marburg virus entry inhibitors. *Antimicrob Agents Chemother* 2016;**60**:4471-81.

26 Pu SY, Xiao F, Schor S, Bekerman E, Zanini F, Barouch-Bentov R, et al. Feasibility and biological rationale of repurposing sunitinib and erlotinib for dengue treatment. *Antiviral Res* 2018;**155**:67-75.

27 Schornberg K, Matsuyama S, Kabsch K, Delos S, Bouton A, White J. Role of endosomal cathepsins in entry mediated by the Ebola virus glycoprotein. *J Virol* 2006;**80**:4174-8.

28 Barrientos LG, Rollin PE. Release of cellular proteases into the acidic extracellular milieu exacerbates Ebola virus-induced cell damage. *Virology* 2007;**358**:1-9.

29 van der Linden WA, Schulze CJ, Herbert AS, Krause TB, Wirchnianski AA, Dye JM, et al. Cysteine cathepsin inhibitors as anti-Ebola agents. *ACS Infect Dis* 2016;**2**:173-9.

30 Lu F, Liang Q, Abi-Mosleh L, Das A, De Brabander JK, Goldstein JL, et al. Identification of NPC1 as the target of U18666A, an inhibitor of lysosomal cholesterol export and Ebola infection. *Elife* 2015;**4**:e12177.

31 Basu A, Mills DM, Mitchell D, Ndungo E, Williams JD, Herbert AS, et al. Novel small molecule entry inhibitors of Ebola virus. *J Infect Dis* 2015;**212 Suppl 2**:S425-34.

32 García-Dorival I, Cuesta-Geijo MÁ, Barrado-Gil L, Galindo I, Garaigorta U, Urquiza J, et al. Identification of Niemann-Pick C1 protein as a potential novel SARS-CoV-2 intracellular target. *Antiviral Res* 2021;**194**:105167.

33 Wang LL, Palermo N, Estrada L, Thompson C, Patten JJ, Anantpadma M, et al. Identification of filovirus entry inhibitors targeting the endosomal receptor NPC1 binding site. *Antiviral Res* 2021;**189**:105059.

34 Ren J, Zhao Y, Fry EE, Stuart DI. Target identification and mode of action of four chemically divergent drugs against Ebolavirus infection. *J Med Chem* 2018;**61**:724-33.

35 Zhao Y, Ren J, Fry EE, Xiao J, Townsend AR, Stuart DI. Structures of Ebola virus glycoprotein complexes with tricyclic antidepressant and antipsychotic drugs. *J Med Chem* 2018;**61**:4938-45.

36 Zhao Y, Ren J, Harlos K, Jones DM, Zeltina A, Bowden TA, et al. Toremifene interacts with and destabilizes the Ebola virus glycoprotein. *Nature* 2016;**535**:169-72.

37 Li Q, Ma L, Yi D, Wang H, Wang J, Zhang Y, et al. Novel cyclo-peptides inhibit Ebola pseudotyped virus entry by targeting primed GP protein. *Antiviral Res* 2018;**155**:1-11.

38 Bray M, Davis K, Geisbert T, Schmaljohn C, Huggins J. A mouse model for evaluation of prophylaxis and therapy of Ebola hemorrhagic fever. *J Infect Dis* 1998;**178**:651-61.

39 Wang Y, Cui R, Li G, Gao Q, Yuan S, Altmeyer R, et al. Teicoplanin inhibits Ebola pseudovirus infection in cell culture. *Antiviral Res* 2016;**125**:1-7.

40 Li Q, Liu Q, Huang W, Li X, Wang Y. Current status on the development of pseudoviruses for enveloped viruses. *Rev Med Virol* 2018;**28**:e1963.

41 Trott O, Olson AJ. AutoDock Vina: improving the speed and accuracy of docking with a new scoring function, efficient optimization, and multithreading. *J Comput Chem* 2010;**31**:455-61.

42 O'Boyle NM, Banck M, James CA, Morley C, Vandermeersch T, Hutchison GR. Open babel: an open chemical toolbox. *J Cheminform* 2011;**3**:33.

43 Hou T, Wang J, Li Y, Wang W. Assessing the performance of the MM/PBSA and MM/GBSA methods. 1. The accuracy of binding free energy calculations based on molecular dynamics simulations. *J Chem Inf Model* 2010;**51**:69-82.

44 Sakurai Y, Kolokoltsov AA, Chen CC, Tidwell MW, Bauta WE, Klugbauer N, et al. Ebola virus. Two-pore channels control Ebola virus host cell entry and are drug targets for disease treatment. *Science* 2015;**347**:995-8.

45 Song XY, Kong LL, Chen NH. Berbamine. In: Du GH, Editor. *Natural small molecule drugs from plants*. Singapore: Springer Singapore; 2018. p 485-9.

46 O'Hearn A, Wang M, Cheng H, Lear-Rooney CM, Koning K, Rumschlag-Booms E, et al. Role of EXT1 and glycosaminoglycans in the early stage of filovirus entry. *J Virol* 2015;**89**:5441-9.

47 Saeed MF, Kolokoltsov AA, Albrecht T, Davey RA. Cellular entry of Ebola virus involves uptake by a macropinocytosis-like mechanism and subsequent trafficking through early and late endosomes. *PLoS Pathog* 2010;**6**:e1001110.

48 Nanbo A, Imai M, Watanabe S, Noda T, Takahashi K, Neumann G, et al. Ebolavirus is internalized into host cells *via* macropinocytosis in a viral glycoprotein-dependent manner. *PLoS Pathog* 2010;**6**:e1001121.

49 Cavrois M, De Noronha C, Greene WC. A sensitive and specific enzyme-based assay detecting HIV-1 virion fusion in primary T lymphocytes. *Nat Biotechnol* 2002;**20**:1151-4.

50 Guo N, Peng Z. MG132, a proteasome inhibitor, induces apoptosis in tumor cells. *Asia Pac J Clin Oncol* 2013;**9**:6-11.

51 Hashiguchi T, Fusco ML, Bornholdt ZA, Lee JE, Flyak AI, Matsuoka R, et al. Structural basis for Marburg virus neutralization by a cross-reactive human antibody. *Cell* 2015;**160**:904-12.

52 King LB, Fusco ML, Flyak AI, Ilinykh PA, Huang K, Gunn B, et al. The marburgvirus-neutralizing human monoclonal antibody MR191 targets a conserved site to block virus receptor binding. *Cell Host Microbe* 2018;**23**:101-9.e4.

53 Chang HM, But PP. *Pharmacology and applications of Chinese materia medica*. Vol. 1. Singapore: World Scientific Pub. Co.; 1986.

Figure captions

Figure 1 Identification of EEI-10 as an EBOV entry inhibitor. (A) The receptor binding region identified in GPcl (PDB ID 5F1B). Left, the structure of the GPcl (yellow) in complex with NPC1 (green). Right, the receptor binding cavity at the top of GPcl. Highlighted in magenta is residues that constitute the interaction interface and are targeted by the virtual screening. (B) The virtual screening strategy designed to identify small molecules targeting GPcl. (C) Chemical structure of EEI-10, with molecule weight (MW). (D) Representative association and dissociation sensorgrams of EEI-10 binding to EBOV-GPcl. Values of K_D and K_D error are presented. Data shown represent three independent experiments. The values are expressed as means ± SD. (E, F) GST pull-down assay was applied to characterize the interaction between GPcl and NPC1-C in the presence of EEI-10 or TET. GPcl-His was primarily mixed with EEI-10 or TET (10, 50, and 250 μmol/L) for 1 h at 4 °C before adding GST-NPC1-C protein. (G) HEK293T cells were infected with the EBOVpp in the presence of EEI-10 at the final concentration of 10 μmol/L. VSVpp was used to control the specific antiviral effect of the tested drugs. Data are normalized to that of the control group (arbitrarily set as 1). (H) Does-depended inhibition of EBOVpp by EEI-10 or TET. (I) Inhibition of EBOV infection of Vero E6 cells by EEI-10 of different doses. Each data point is the average of three independent experiments. EC_{50} values were calculated with GraphPad Prism 5.0. All data shown above are mean ± SD ($n = 3$), if not otherwise specified. $^{*}P < 0.05$, $^{***}P < 0.001$ compared to control.

Figure 2 EEI-10 inhibits EBOV-GP-dependent virus–cell membrane fusion. (A) Time-addition experiment to determine the inhibition mechanism by EEI-10, TET and EFV. (B) Binding test to measure the effect of EEI-10 on virus binding to the cell membrane. Heparin was used as a positive control. Viral RNA from virus particles binding to the cell membrane was quantified by qRT-PCR. Data are normalized to that the control group which is arbitrarily set to 1. (C) Virus particles (red) in the acidic endosomes were scored by their colocalization with LAMP1 (green) (as for Fig. S6). Fluorescence intensity of green and red signals from randomly selected cells ($n \geq 30$) was quantified by Image-Pro Plus 10 software. (D) VLPs (EBOVpp and VSVpp) loaded with BlaM-Vpr were used to measure membrane fusion and virus capsid release into the cytoplasm after EEI-10 and TET treatment by flow cytometry (as for Fig. S7). The bar graph presents the percentages of virus release into the cytoplasm. (E) VLPs (EBOVpp and

VSVpp) accumulated in the cytoplasm after EEI-10 and TET treatment. The number of VLPs (red signals) in confocal images was determined from randomly selected cells ($n \geq 80$). The fluorescence intensity was quantified by Image-Pro Plus 10 software. All data shown above are mean ± SD of three independent experiments. $^{*}P < 0.05$, $^{***}P < 0.001$ compared to control. n.s., not significant.

Figure 3 EEI-10 disrupts the binding of EBOV-GPcl to NPC1. (A) Colocalization of Ebola VLPs with NPC1 was determined by incubating VLPs with HEK293 cells for 4 h. Representative confocal images are shown. Colocalized Ebola VLPs (Green) and NPC1(Red) were indicated by arrowheads. Scale bar, 5 μm. (B) HEK293T cells were exposed to EBOVpp which were treated with protease thermolysin to generate EBOV GPcl, in the presence of EEI-10 or TET. The cysteine protease inhibitor E-64 was used as a positive control. Luciferase activities were measured and normalized to those of untreated controls. (C) Interaction between NPC1-C-Flag and GPcl-His was determined with Co-IP in the presence of EEI-10 or TET. Data shown are the representative of three independent experiments. (D) *In situ* PLA was used to analyze the interaction between EBOV-GP (or VSV-G) and cellular NPC1 in the presence of the EEI-10 or TET. Images were collected from five fields of view per condition per experiment, in which the surface of a total of at least 30 cells were observed. Each data point represents the average fluorescence intensity of cells observed in each field. Representative confocal images are shown. Scale bar, 5 μm. All data shown above are mean ± SD of three independent experiments. $^{***}P < 0.001$ compared to control. n.s., not significant.

Figure 4 EEI-10 inhibits infection mediated by the GPs of EBOV and MARV. (A) Structural model of EEI-10 binding to GPcl. Amino residues (in yellow) binding to EEI-10 (in green) are shown as sticks. The oxygen, nitrogen, and hydrogen atoms are colored in red, blue, and white, respectively. For clarity, only polar hydrogen atoms are shown. The PDB ID of the EBOV-GPcl crystal structure used for molecular modeling is 5F1B. (B) Inhibition of the T83A and I113A GP mutants by EEI-10. Luciferase activities were measured and normalized to those of untreated controls. (C) Inhibition of MARV GP-pseudovirions by EEI-10 of different doses. (D) Different doses of EEI-10 were tested for inhibition of MARV infection in Vero E6 cells. Each data point is the average of three independent experiments. EC_{50} values are calculated with GraphPad

Prism 5.0. (E) Superposition of the structures of the EBOV-GPcl/EEI-10 and MARV-GP1/EEI-10 complexes. EBOV-GPcl and MARV-GP1 are shown as yellow and slate cartoons, and their associate inhibitor EEI-10 was shown as green and orange sticks. (F) Comparison of protein−ligand interactions in the EBOV-GPcl/EEI-10 and MARV-GP1/EEI-10 complexes. Key residues in the MARV-GP1/EEI-10 binding pocket are highlighted in red. The PDB IDs of crystal structures used for molecular modeling are 5F1B for EBOV GPcl and 5UQY for MARV GP1. All data shown above are mean ± SD ($n = 3$), if not otherwise specified. $^{**}P < 0.01$, $^{***}P < 0.001$ compared to control. n.s., not significant.

Figure 5 Single-does PK study in mice showing plasma concentrations of EEI-10 as specified after dosing with EEI-10 (25 mg/kg; *p.o.*). Symbols represent individual biological repeat (n=3), error bars show standard deviations, lines depict sample means.

Figure 6 EEI-10 prevents lethal EBOV infection in mice. (A) Schematic representation of EEI-10 treatment protocol and EBOV infection of mice. (B, C) BALB/c mice were treated orally with EEI-10 (100 mg/kg; $n = 10$) or PBS ($n = 7$) one day before infection with 1000 LD50 mouse-adapted EBOV (MA-EBOV). Treatment continued once daily until Day 6 after infection. Survival (in B) and average percent weight changes ± SD (in C) are shown. (D, E) BALB/c mice were infected with 1000 LD50 MA-EBOV one day prior to oral treatment with EEI-10 (100 mg/kg; $n = 6$) or PBS ($n = 6$). Treatment continued once daily until Day 6 post-infection. Survival (in D) and average percent weight changes ± SD (in E) are shown. Survival curves were compared using the Mantel-Cox (log-rank) test: $^{***}P < 0.001$.